Front. Earth Sci. 2022, 16(1): 132–143
https://doi.org/10.1007/s11707-021-0877-x

RESEARCH ARTICLE

Predictability and dynamics of the rapid intensification of Super Typhoon Lekima (2019)

Mengting XU[1,2], Hong LI (✉)[1,2], Jingyao LUO[1,2], Hairong BEN[3], Yijie ZHU[1,2]

1 Shanghai Typhoon Institute, China Meteorological Administration, Shanghai 200030, China
2 Key Laboratory of Numerical Modeling for Tropical Cyclones, China Meteorological Administration, Shanghai 200030, China
3 Taizhou Meteorological Bureau, Taizhou 318000, China

Abstract This study explores the effect of the initial axisymmetric wind structure and moisture on the predictability of the peak intensity of Typhoon Lekima (2019) through a 20-member ensemble forecast using the WRF model. The ensemble members are separated into Strong and Weak groups according to the maximum 10-m wind speed at 48 h. In our study of Lekima (2019), the initial intensity defined by maximum 10-m wind speed is not a good predictor of the intensity forecast. The peak intensity uncertainty is sensitive to the initial primary circulation outside the radius of maximum wind (RMW) and the initial secondary circulation. With greater absolute angular momentum (AAM) beyond the RMW directly related to stronger primary circulation, and stronger radial inflow, Strong group is found to have larger AAM import in low-level, helping to spin up the TC. Initial moisture in inner-core is also critical to the intensity predictability through the development of inner-core convection. The aggregation and merger of convection, leading to the TC intensification, is influenced by both radial advection and gradient of system-scale vortex vorticity. Three sensitivity experiments are conducted to study the effect of model uncertainty in terms of model horizontal grid resolution on intensity forecast. The horizontal grid resolution greatly impacts the predictability of Lekima's intensity, and the finer resolution is helpful to simulate the intensification and capture the observed peak value.

Keywords tropical cyclone, intensity, predictability, rapid intensification, initial condition, model resolution

Received July 8, 2020; accepted February 7, 2021

E-mail: lih@typhoon.org.cn

1 Introduction

Tropical cyclones (TCs) often cause serious damage, leading to injury or death (Chen et al., 2019; Yu and Chen, 2019). Although the technology of TC track forecast has been improved dramatically in the last decade, little improvement of TC intensity forecast has been made (DeMaria et al., 2014), especially for TCs with rapid intensification (RI). In this paper, we focus on Super Typhoon Lekima (2019), which is the fifth intense typhoon landfalling Chinese mainland since 1949. It underwent a RI process, intensifying from a typhoon with maximum wind speed of 33 m/s at 1800 UTC 6 August, to super-typhoon with maximum wind speed of 62 m/s at 1200 UTC 8 August, over a 42-h period. Almost all operational forecasting systems failed to forecast the peak intensity. The current study will examine sources of forecast uncertainties and errors, which limit the predictability of this RI event of typhoon Lekima.

To improve TC modeling forecast, it is useful to be aware of intrinsic and practical predictability limits caused by the inherent chaotic nature of TC and limitation of current numerical prediction. The intrinsic predictability of TC intensity is affected by external and internal factors. Many previous studies have paid attention to the roles of external (environmental) factors, such as sea surface temperature (Tao and Zhang, 2014) and vertical wind shear (Zhang and Tao, 2013; Tao and Zhang, 2015; Ryglicki et al., 2018). However, numerous studies have pointed out that internal processes (i.e., inner-core TC dynamics) may also be critical to the predictability of TC intensity, e.g., the initial intensity of vortex (Munsell et al., 2017; Liu et al., 2018; Nystrom et al., 2018), the initial size of vortex (Xu and Wang, 2010; Chen et al., 2011; Carrasco et al., 2014; Guo and Tan, 2017), and the inner-core evolution (Nguyen et al., 2008; Zhang and Sippel, 2009; Rogers, 2010; Liu et al., 2018).

The practical predictability is more complicate and lower. Besides the intrinsic limit, related to the chaotic nature of TC, other key factors limiting the practical predictability include: initial condition (IC) uncertainty and model uncertainty. The former is impacted by data assimilation methods and the assimilated observations, the latter includes model resolution, model physics, air-sea interaction (Berner et al., 2015; Andreas et al., 2016; Nystrom and Zhang, 2019), etc.

Initial wind structure (e.g., maximum 10-m wind speed, primary and secondary circulation) are proved to be an important factor to intensity forecast. With a series of sensitivity experiments, Nystrom et al. (2018) demonstrated that the initial intensity in terms of maximum wind speed is a good predictor of the intensity forecast, as members with stronger initial intensity generally intensify. The initial primary and secondary circulations beyond the radius of maximum wind (RMW) in the inner-core are identified as the dominant sources of initial condition uncertainty impacting the predictability of peak intensity in Nystrom and Zhang (2019). Besides the initial TC vortex intensity, inner-core moisture is also regarded as a crucial factor to the predictability of TC intensity in Liu et al. (2018). Nystrom et al. (2018) indicated that ensemble members with higher relative humidity (RH) near the surface leading to stronger forecast intensity through stronger convection. Based on these we would assess whether the IC uncertainty in terms of wind structure (e.g., maximum wind speed, primary and secondary circulation) and moisture are sensitivity to the predictability of the Lekima's RI process in this study.

Many previous studies (Gentry and Lackmann, 2010; Jin et al., 2014; Roberts et al, 2020; Vannière et al., 2020) have revealed that fine resolution can improve tropical cyclone intensity predictability. The statistical analyses in Jin et al. (2014) indicate that high resolution can improve TC intensity and structure forecasts through several factors such as greater fine-scale structure associated with deep convection, including spiral rainbands and the secondary circulation. It seems that finer resolution would simulate finer structure, which is crucial to the TC intensification.

TCs would not intensify without organized deep convection bursts, in spite of all the environmental factors being advantageous (Gray, 1998). The genesis and intensification of TCs are related to the aggregation and merger of the small-scale vorticity anomalies (Montgomery et al., 2006), which would be regulated by the gradient of system-scale vortex vorticity (Ge et al., 2013; Xu et al., 2016). Convection inside the RMW is in favor of TC intensification (Rogers, 2010), due to the larger inertial stability (Rogers et al., 2016; Wang and Heng, 2016). The importance of convection to TC intensifying is undisputed. Thus, it would be necessary to explore how the processes of convection related to the initial condition uncertainty.

Among these various factors, the IC uncertainty associated with inner-core TC dynamics (e.g., primary and secondary circulation, moisture) and model error in terms of horizontal resolution are assessed in this study to investigate their impacts on the RI of Lekima. The inner-core here covers the area inside a radius of three times the radius of maximum wind (RMW) (Wang, 2009).

Section 2 describes the methodology used in this study. Section 3 compares the ensemble forecasts and examines the sensitivity of Lekima's intensification to initial condition in the inner-core region. Sensitivity experiments with different model horizontal resolutions are conducted in Section 4. Finally, the main findings are summarized and discussed in Section 5.

2 Method

The deterministic and 20-member ensemble forecasts for Lekima are produced by utilizing the Advanced Research core of the Weather Research and Forecasting (ARW-WRF) model (version 3.9.1) (Skamarock and Coauthors, 2008). The model is configured with three two-way nested domains with horizontal grid spacing of 27, 9, and 3 km in domains d01, d02, and d03 (details can be found in supplementary material). The lateral boundary and initial conditions pre-processed into the WRF model for the deterministic forecast are from the NCEP Global Forecast System (GFS) $0.5°\times0.5°$ analysis. The initial ensemble perturbations are gained by subtracting each ensemble member of the NCEP Global Ensemble Forecast System (GEFS) $1.0°\times1.0°$ products from their mean and then added to the deterministic to form the 20-member initial conditions. We apply the Yonsei University scheme (Hong et al., 2006) for planetary boundary layer process, the WSM 6-class graupel microphysics scheme (Hong et al., 2004), and the thermal diffusion land surface scheme. The KF (new Eta) cumulus scheme (Kain and Fritsch, 1993) is applied only to the outermost domain (d01).

To better understand forecast sensitivity to ICs, ensemble forecasting is utilized to explore the ICs error growth. The ensemble experiments are initialized at 0000 UTC 06 August and run for 60-h till 1800 UTC 08 August, covering the entire period of Lekima's RI process. The methodology employed in Sippel and Zhang (2008) and Munsell et al. (2017) is used to separate ensemble members and create two composite groups based on their forecasted peak intensity.

3 Results and discussion

3.1 Ensemble simulations and sensitivity analysis of initial intensity

The evolution of intensity is shown in terms of maximum 10-m wind speed in Fig. 1. The best track data from China Meteorological Administration (Ying et al., 2014) is used

to compare. The intensity is predicted well by ensemble members during the first 24 h, while most of members underestimate the rate of intensification beyond ~30 h and fail to capture the peak intensity at 60 h. However, there are still some members that successfully reach the peak intensity. It might be worth exploring the difference between the successful predicted and failed predicted ensemble members in further detail and diagnosing the factors affecting the predictability of the RI.

The ensemble members are separated into Strong (the 3 strongest members) and Weak (the 3 weakest members) groups according to the maximum 10-m wind speed at 48 h. As seen in Fig. 1, the initial maximum 10-m wind speed is random across the ensemble members and is not well correlated to the final forecast intensity, i.e., members with initially stronger (weaker) maximum 10-m wind do not necessarily result in ultimately stronger (weaker) intensity. It suggests that the initial intensity defined by maximum 10-m wind speed is not a good predictor of the intensity forecast, inconsistent with that of Nystrom et al. (2018), whose viewpoint is that the initial intensity is a strong determining factor in the maximum intensity.

3.2 Impact of initial wind structure on Lekima's intensification

The storm-relative azimuthal mean wind structure is exhibited to explore how the TC initial wind structure uncertainty related to the forecast of peak intensity Fig. 2. The biggest differences between Strong and Weak members' primary circulation are found to be beyond the RMW (Fig. 2(c)) in low and middle levels. We hypothesize that, for the initial primary circulation, it is the difference in the region outside the RMW rather than at the RMW, which contributes the divergence of intensification of ensemble members in Lekima. Stronger tangential winds outside the RMW lead to larger peak intensity. In regards to the secondary circulation (Figs. 2(d)–2(f)), the low-level inflow in Strong is not only deeper but also stronger than in Weak at the vicinity of RMW. The upper-level outflow in Strong is significantly larger than in Weak. In a word, the initial stronger secondary circulation is leading to stronger peak intensity.

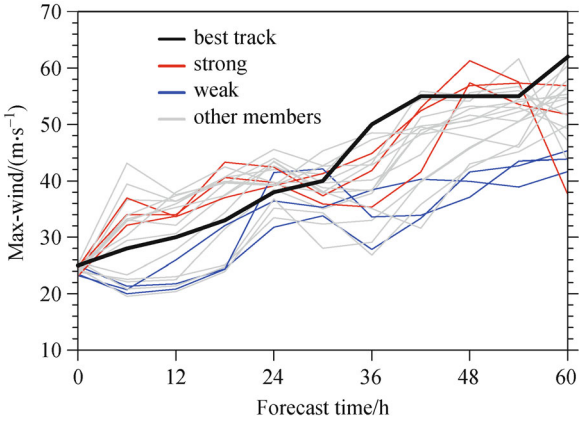

Fig. 1 The 20-member ensemble forecast of maximum 10-m wind speed. Ensemble members are colored according to their intensity at 48 h.

To further explore the relationship between the TC initial wind structure and maximum intensity, azimuthal mean correlations are calculated between the initial wind fields and maximum 10-m wind speed at 48 h.

The positive correlations between the initial tangential wind speed at initial time and the intensity (maximum 10-m wind speed) at 48 h do not occur at the RMW, but rather outside the RMW at the low and middle levels (Fig. 3(a)). The statistically significant positive correlations appear at 3–6 km and 9–11 km, the similar region confirmed by the largest ensemble differences in Fig. 2(c).This reveals that ensemble members with more intense initial primary circulation outside the RMW are more likely to reach stronger intensity at 48 h, consistent with the conclusions in Nystrom and Zhang (2019).

The initial secondary circulation also exhibits significant relationship with the maximum 10-m wind speed at 48 h. Negative correlations, absolute value larger than 0.4, inside the radius of 270 km within the lowest 4 km (Fig. 3(b)), reveal that stronger initial low-level inflow is associated with a more intense TC at 48 h. Meanwhile, positive correlations at upper-levels, indicate that ensemble members with stronger initial outflow are more likely to reach stronger intensity at 48 h. Stronger inflow and outflow are usually related to stronger Ekman pumping, leading to stronger intensity. Overall, it seems that the initial primary circulation beyond the RMW and the initial secondary circulation are two of determining factors of the peak intensity.

Previous studies (Chen et al., 2011; Chan and Chan, 2013) have indicated that the absolute angular momentum (AAM) import from the outer region is a significant contributor to TC intensification. A large AAM import is beneficial for increasing inner-core wind and the TC intensification. The radial transport of AAM depends on the product of the low-level radial inflow (associated with radial wind) and the AAM at a certain radius of TC (associated with tangential wind). The biggest differences of AAM between Strong and Weak (Fig. 4(a)) are outside the RMW in low and middle levels, in agreement with the tangential wind difference (Fig. 2(c)). It is displayed in Fig. 4(b) that stronger AAM exports to the outer region in upper-level and larger AAM imports to the TC center in low-level in the Strong group, increasing wind speeds near the RMW and favoring the formation of an intense TC.

3.3 Impact of initial moisture on Lekima's intensification

Previous studies (Nguyen et al., 2008; Emanuel and Zhang, 2017; Liu et al., 2018) have emphasized the vital function of inner-core moisture to TC intensification through deep convective bursts. In this subsection, we

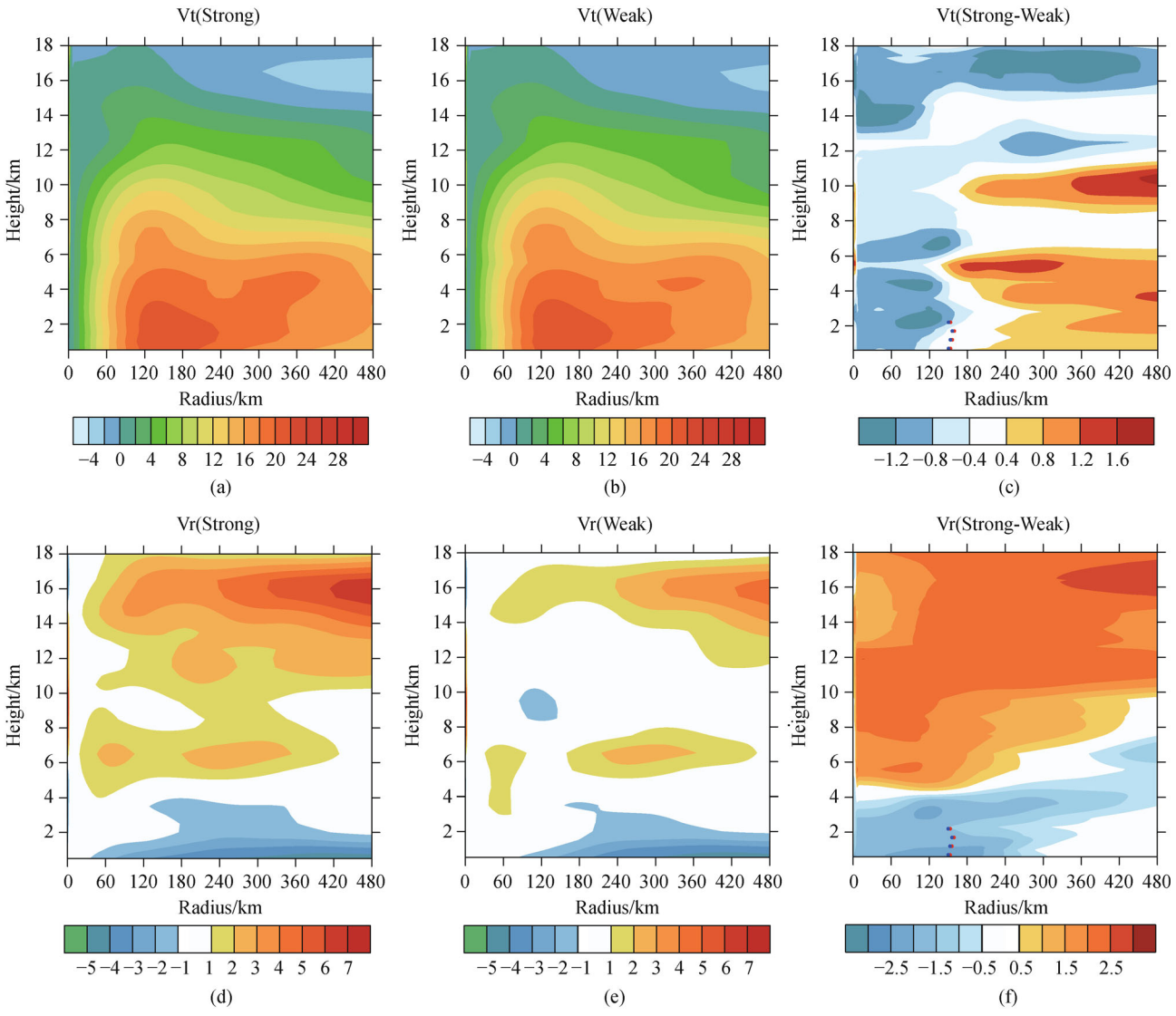

Fig. 2 The initial (T = 0 h) radius-height plots of axisymmetric tangential wind speed (a) in Strong (shaded, units: m/s), (b) in Weak (shaded, units: m/s), and (c) difference between Strong and Weak (shaded, units: m/s). The initial (T = 0 h) radius-height plots of axisymmetric radial wind speed (d) in Strong (shaded, units: m/s), (e) in Weak (shaded, units: m/s), and (f) difference between Strong and Weak (shaded, units: m/s). The dots in (c) and (f) denotes the RMW (red: Strong, blue: Weak).

would like to examine the relationship between the initial moisture condition and the peak intensity.

At the initial time, the largest azimuthal mean water vapor mixing ratio (QVAPOR) occurs in the lowest level inside the RMW in both Strong (Fig. 5(a)) and Weak (Fig. 5(b)) groups. The normalized differences of the initial moisture structure between Strong and Weak show a large area of positive values everywhere below ~10 km, across nearly the entire inner-core (Fig. 5(c)). In addition, the largest positive correlations (Fig. 5(d)) between initial azimuthal mean QVAPOR and maximum 10-m wind speed at 48 h locate in the same region as the initial difference between Strong and Weak (Fig. 5(c)), indicating that more abundant initial moisture corresponds to stronger TC intensity at 48 h.

A small, random initial moisture perturbation in the boundary layer can influence the final intensity through deep convective bursts (Nguyen et al., 2008). Thus, it is necessary to analyze the evolution of convection. The composited reflectivity of Strong and Weak groups at the height of 3 km are shown in Fig. 6 to display the development of convection in the inner-core. Due to more sufficient initial water vapor (Fig. 5), the convection in Strong is more vigorous than that in Weak at the early phase (T = 12 h). The convection in Strong is much more organized and stronger than that in Weak in the following forecast times, and the difference increases over time. Eventually, there is a closed eyewall at 48 h in Strong, corresponding to stronger intensity. Moreover, aggregation and merger of convection, related to the intensification of

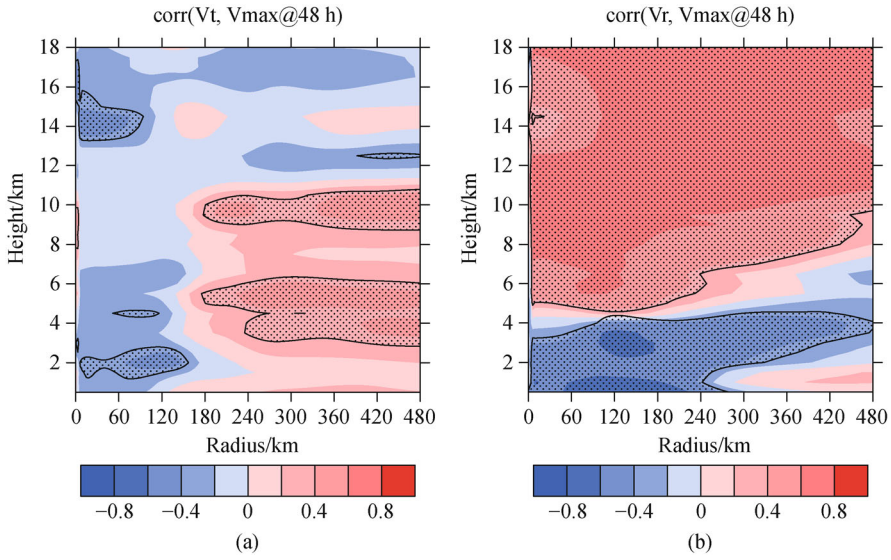

Fig. 3 Ensemble azimuthal mean radius-height correlations between initial (a) tangential wind speed, (b) radial wind speed and the maximum 10-m wind speed at 48 h. Stippling denotes regions where the statistical significance exceeds the 99% confidence interval.

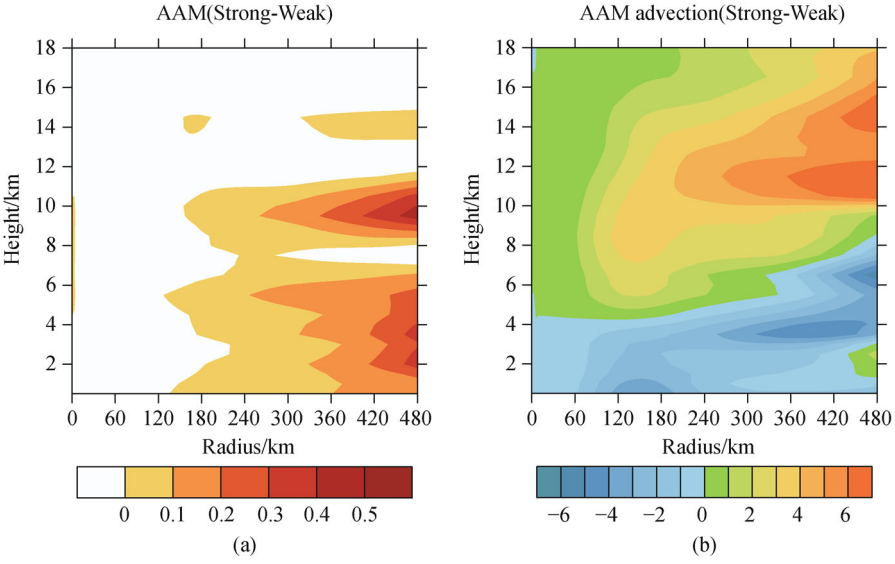

Fig. 4 The initial ($T = 0$ h) radius-height plots of the difference of (a) axisymmetric absolute angular momentum (AAM) (shaded, units: 10^6 m^2/s) between Strong and Weak, and (b) axisymmetric AAM radial advection (shaded, units: 10^6 m^3/s^2) between Strong and Weak.

TC, is observed in both Strong and Weak. We hypothesize that there are two mechanism accounting for the aggregation and merger of convection, one is radial advection and the other is vorticity segregation (Schecter and Dubin, 1999; Ge et al., 2013; Xu et al., 2016), which will be explored in the next subsection.

3.4 Evolution of the two groups: Strong and Weak

The impacts of the initial conditions on the TC vortex evolution are investigated in this subsection. Evolution of the azimuthal mean surface tangential wind (at 10 m) and surface heat flux of Strong and Weak groups are exhibited in Figs. 7(a) and 7(b), while evolution of the azimuthal mean surface radial wind (at 10 m) and convection of Strong and Weak groups are shown in Figs. 7(c) and 7(d). Larger and more intensive radial winds, sustaining the radial advection of convection and resulting in more intense inward AAM advection, are observed in Strong (Fig. 7(c)) than in Weak (Fig. 7(d)) at every forecast time. The surface tangential wind in Strong (Fig. 7(a)) is markedly larger and more intensive than those in Weak (Fig. 7(b)) after the initial time, probably due to the greater AAM advection, as mentioned above in Section 3.2. The faster contracting RMW in Strong group is beneficial to TC rapid intensification (Rogers 2010; Xu and Wang, 2010).

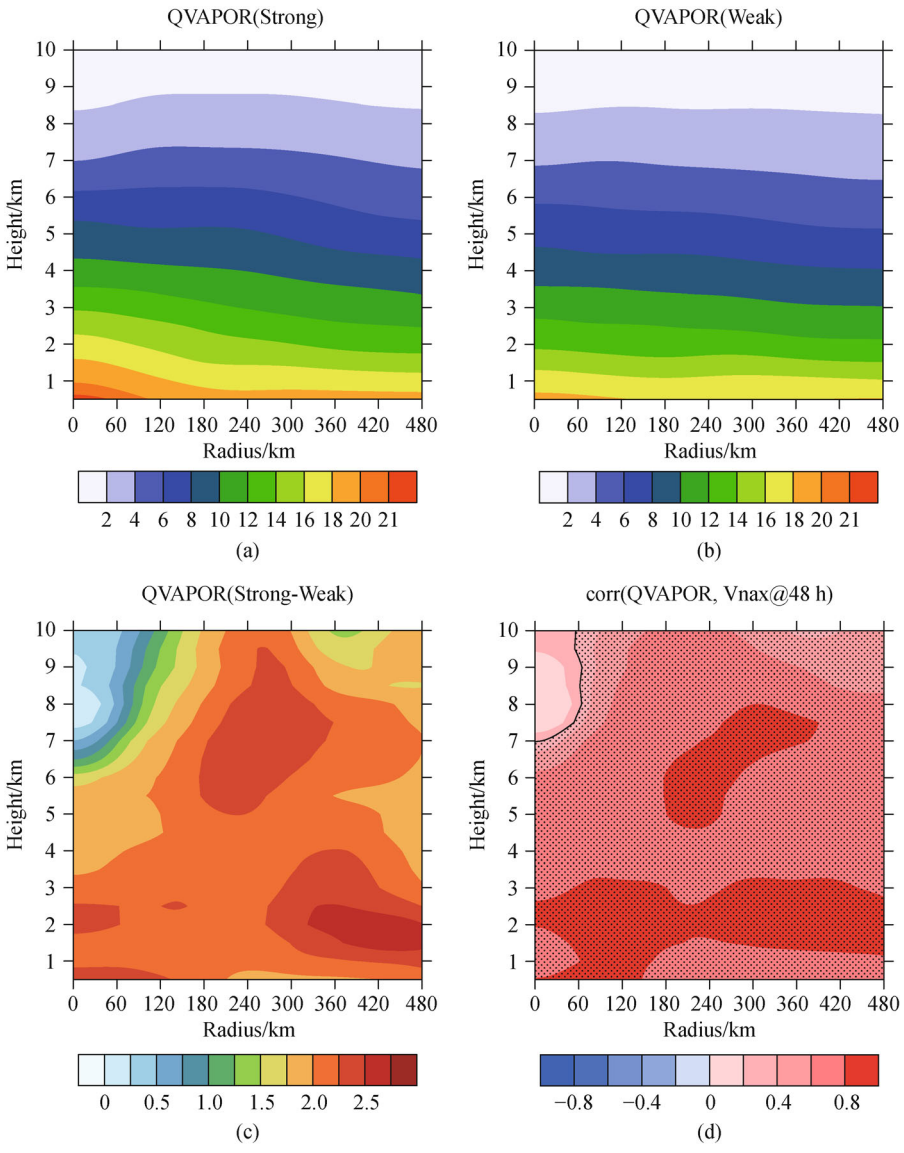

Fig. 5 The initial (T = 0 h) radius-height plots of axisymmetric QVAPOR (a) in Strong (shaded, units: g/kg), (b) in Weak (shaded, units: g/kg), and (c) difference between Strong and Weak (shaded, units: g/kg). (d) Azimuthal mean radius-height correlations between initial QVAPOR and the maximum 10-m wind speed at 48 h. Stippling denotes regions where the statistical significance exceeds the 99% confidence interval in (d).

Moreover, larger surface heat flux in Strong, associated with stronger surface wind and/or surface heat, propagates inward with time, which would help to spin up the TC.

The convection in inner-core in Strong (Fig. 7(c)) is significantly more vigorous and organized than in Weak (Fig. 7(d)) during the whole forecast time, consistent with Fig. 6. Furthermore, there are more convection inside the RMW in Strong group during the first 24 h, being in favor of TC intensification due to the larger inertial stability (Rogers et al., 2016; Wang and Heng, 2016).

Besides the impact of radial advection, gradient of vortex vorticity could influence the aggregation and merger of convection as well, i.e., small-scale vorticity anomalies (e.g., deep convective bursts) would be regulated by the gradient of system-scale vortex vorticity. To be more specific, cyclonic vorticity anomalies tend to move inward the vortex center to increasing the ambient vorticity and thus upscale cascade from small-scale to system-scale, while anticyclonic vorticity anomalies tend to move down the gradient of the ambient vorticity, i.e., vorticity segregation (Schecter and Dubin, 1999). Thus, a spatial filter technique is applied to segregate the small-scale (wavelength less than 100 km) component and system-scale component (wavelength larger than 100 km) to analyze the phenomenon of aggregation and merger of convection.

The horizontal distribution of small-scale vorticity and system-scale vorticity at the height of 0.5 km from 12 to 48 h (interval of 12 h) in both Strong and Weak groups are

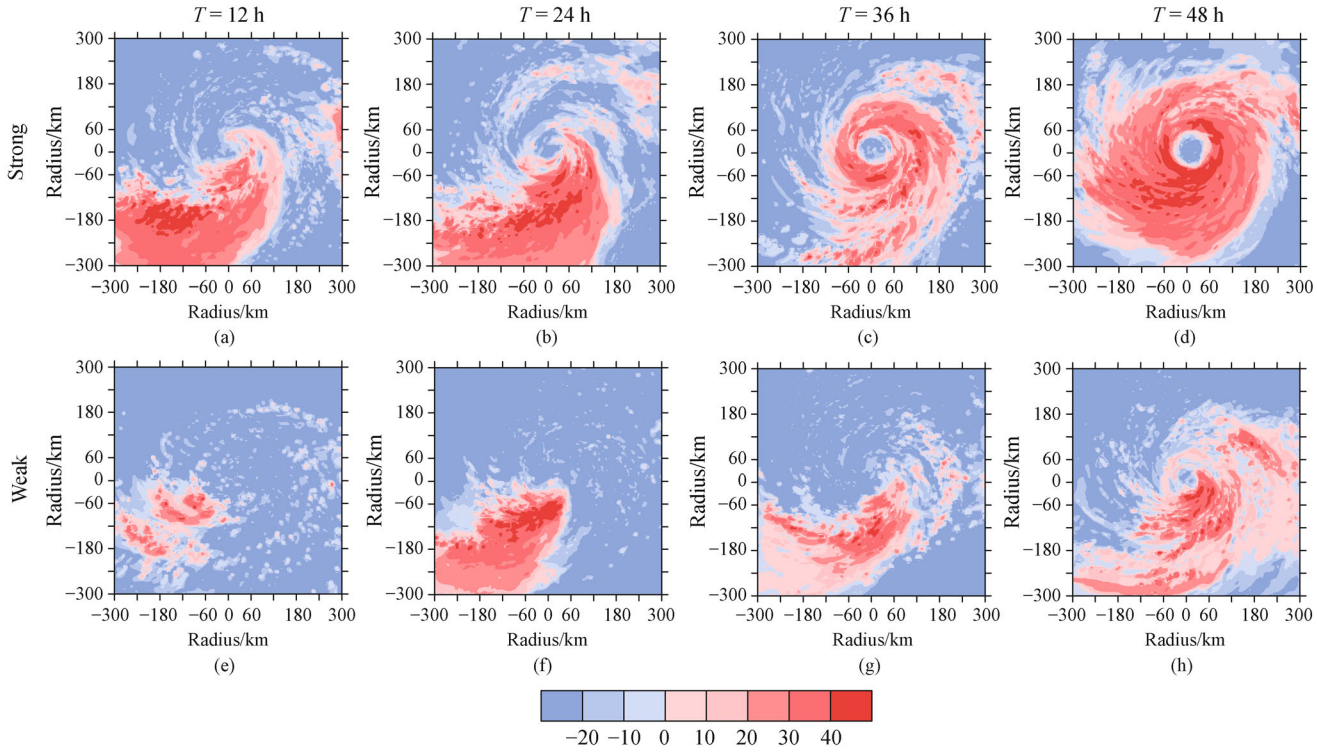

Fig. 6 Composite reflectivity (units: dBZ) of (a–d) Strong and (e–h) Weak at 3 km. (a) and (e) at 12 h, (b) and (f) at 24 h, (c) and (g) at 36 h, (d) and (h) at 48 h.

shown in Fig. 8. It is obvious that the small-scale convections in both groups are collecting and merging ceaselessly as time goes on. The gradient of system-scale vorticity in Strong is denser than in Weak, yield to more intensive tangential wind and radial wind in the inner-core. Denser gradient of system-scale vorticity is more conducive to the aggregation and merger of the small-scale vorticity anomalies. Beyond that, the system-scale vorticity in Strong is significant lager than in Weak at 48 h, which is representing stronger TC intensity.

4 Sensitivity of Lekima's forecasts to model horizontal resolution

In this subsection, we would like to turn our attention to the impact of model error on the predictability of Lekima's intensification. In particularly, we focus on model resolution.

Three experiments are designed with the horizontal resolutions of 27 km (EXP_27), 27/9 km (EXP_9), 27/9/3 km (EXP_3), respectively. The domains applied in these three experiments (more details can be found in supplementary material) are d01, d01/d02, d01/d02/d03, respectively. As shown in Fig. 9, the peak intensity in terms of the maximum 10-m wind speed in EXP_3 is the strongest, 63 m/s at 60 h and is a little stronger than the best-track (62 m/s), while the values are 51 m/s in EXP_9 and 42 m/s in EXP_27. The intensity forecast error in EXP_3 has been reduced by 90% compared to EXP_9, and 95% to EXP_27, demonstrating the positive effect of improving resolution on intensity forecast.

The maximum 10-m wind speed in EXP_27 is much smaller than those in EXP_9, EXP_3 and best-track along all the forecast times and the significant gap occurs after 48 h. The obvious discrepancy between EXP_3 and EXP_9 also appears after 48 h. The impact of model resolution on the predictability of Lekima's intensity becomes significant large when observed intensity is greater than 40 m/s in the current simulations.

To get more detailed understanding of these three experiments, the storm-relative azimuthal mean structure of tangential wind at 24 h, 48 h and 60 h are displayed in Fig. 10. Due to the finer resolution, the RMWs in EXP_3 and EXP_9 are smaller than in EXP_27. At 36 h and 48 h, there are no big differences among the three experiments. However, at 60 h, both the tangential wind and the radial wind in EXP_27 are smaller than those in EXP_3 and EXP_9. There is no significant difference in regarding to radial wind between EXP_3 and EXP_9, while the maximum tangential wind in EXP_3 is the largest among the three simulations at 60 h, indicating more of AAM beyond RMW may have been transported to the primary circulation to enhance the wind speed at the RMW. Horizontal distribution of 10-m wind speeds indicates that the maximum wind is the largest in EXP_3 (Fig. 11(c)),

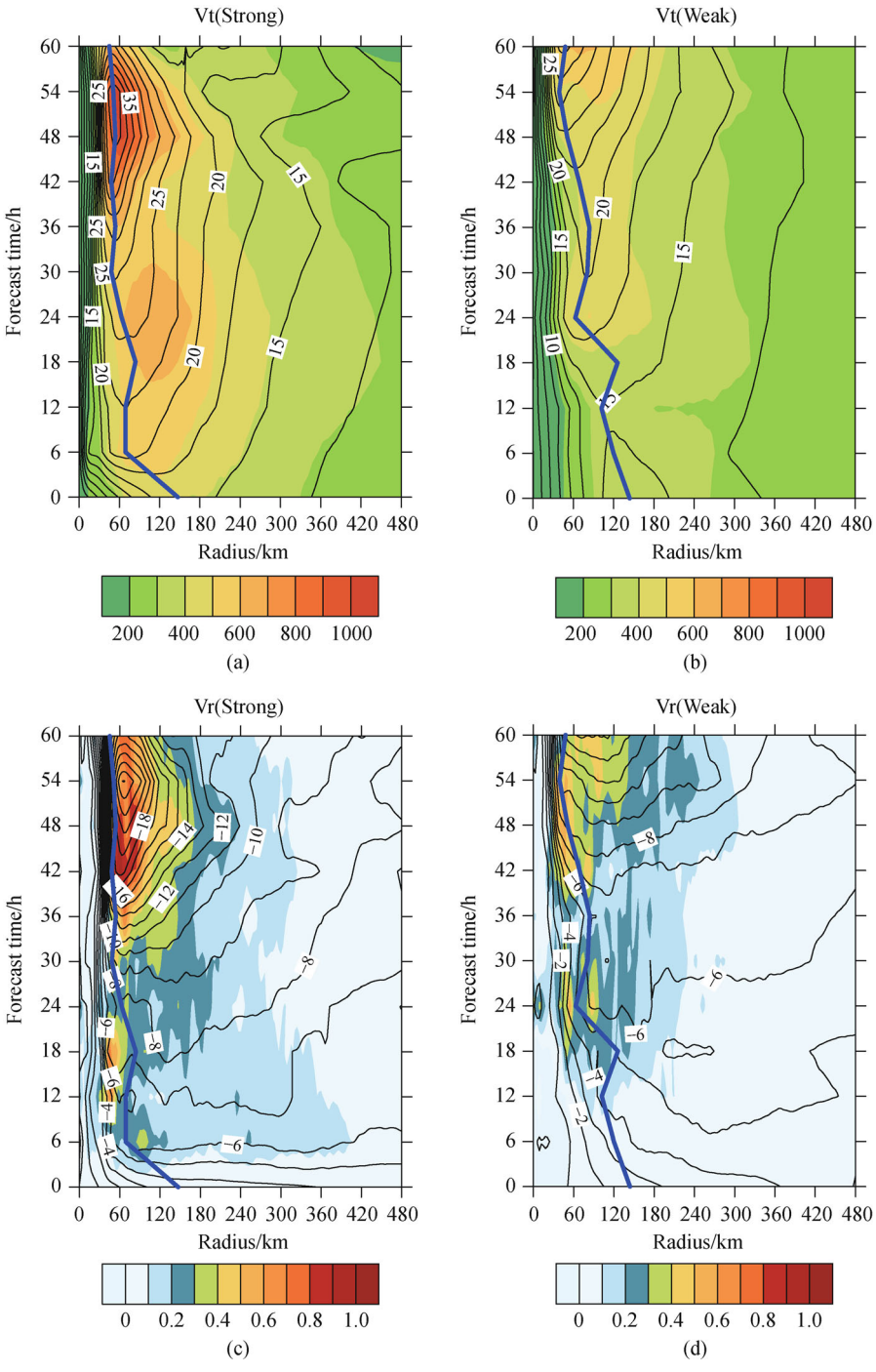

Fig. 7 Evolution of the azimuthal mean 10-m tangential wind (contoured, units: m/s) and surface heat flux (shaded, units: W/m^2) in (a) Strong and (b) Weak. Evolution of the azimuthal mean 10-m radial wind (contoured, units: m/s) and the azimuthal mean vertical wind at 5−15 km (shaded, units: m/s) in (c) Strong and (d) Weak.

~ 60 m/s, which is less than 55 m/s in EXP_9 (Fig. 11(b)) and is less than 45 m/s in EXP_27 (Fig. 11(a)). Meanwhile, the vortex structure in EXP_3 (Fig. 11(c)), is more compact and the radial gradient of horizontal wind is extremely larger than the other two experiments, with 10-m winds increasing more rapidly outside the RMW and decreasing more abruptly inside. Tighter structure leads to stronger intensity. Overall, the model uncertainty in terms of horizontal grid resolution greatly impacts the predictability of Lekima's intensity, and the increased resolution is very important to simulate the intensification and capture the observed peak value.

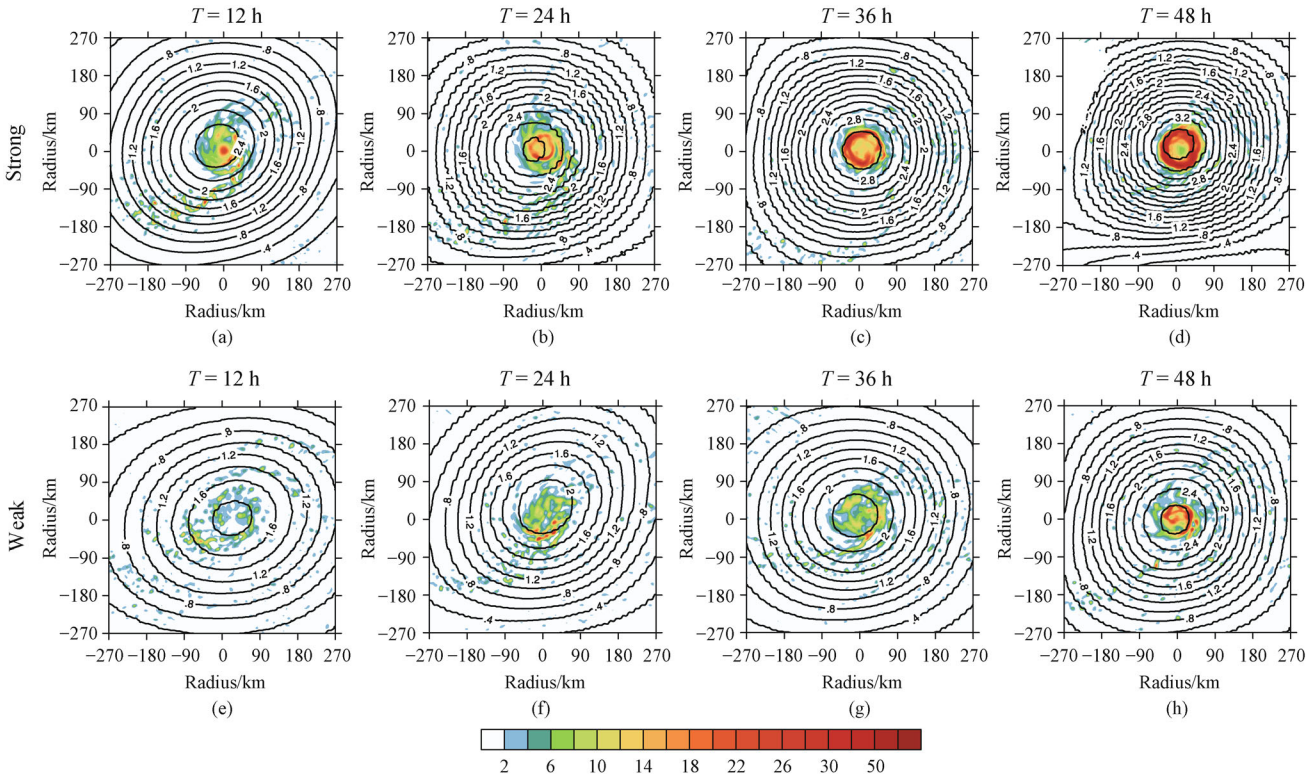

Fig. 8 Horizontal distribution of small-scale vorticity (shaded, units: $10^{-4}\cdot s^{-1}$) and system-scale vorticity (contoured, units: $10^{-4}\cdot s^{-1}$) at the height of 0.5 km from 12 to 48 h (interval of 12 h) in both (a–d) Strong and (e–h) Weak. (a) and (e) at 12 h, (b) and (f) at 24 h, (c) and (g) at 36 h, (d) and (h) at 48 h.

5 Conclusions

This study explores the effect of the initial wind structure and moisture on the predictability of typhoon Lekima's peak intensity through a 20-member ensemble forecast using the WRF model. Some members successfully reach the peak intensity, while the others do not. The ensemble members are separated into Strong (the 3 strongest members) and Weak (the 3 weakest members) groups according to the maximum 10-m wind speed at 48 h to examine the uncertainty in the forecast peak intensity across the ensemble. The uncertainty of model errors also leads to the intensity forecast error. Three additional sensitivity experiments are conducted to study the effect of model uncertainty in terms of model horizontal resolution on intensity forecast errors.

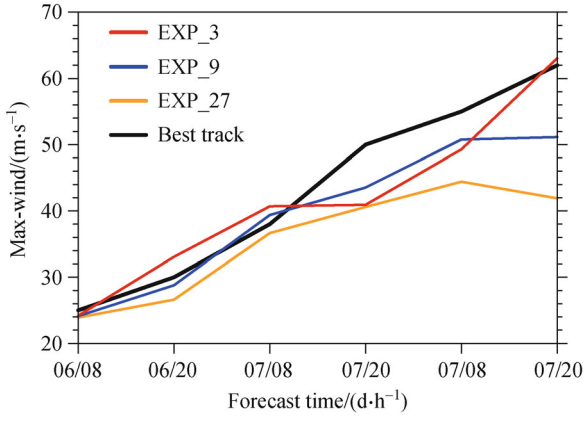

Fig. 9 Evolution of maximum 10-m wind speed for different model resolution simulations.

The maximum 10-m wind speeds at initial time are random across the ensemble members and not well correlated to the forecast final intensity, indicating that the initial intensity defined by maximum 10-m wind speed is not a good predictor of the intensity forecast, inconsistent with that of Nystrom et al. (2018), where the initial intensity is a strong determining factor to the peak intensity.

The initial primary circulation beyond the RMW and the initial secondary circulation are two of determining factors in the peak intensity. The tangential winds beyond the RMW are stronger in Strong than in Weak at the low and middle levels, with significant positive correlations between the initial tangential winds and the maximum 10-m wind at 48 h at the same region. Meanwhile, the radial inflow and outflow in Strong are stronger than in Weak, with significant correlations of the initial radial winds to the maximum 10-m wind at 48 h. Stronger

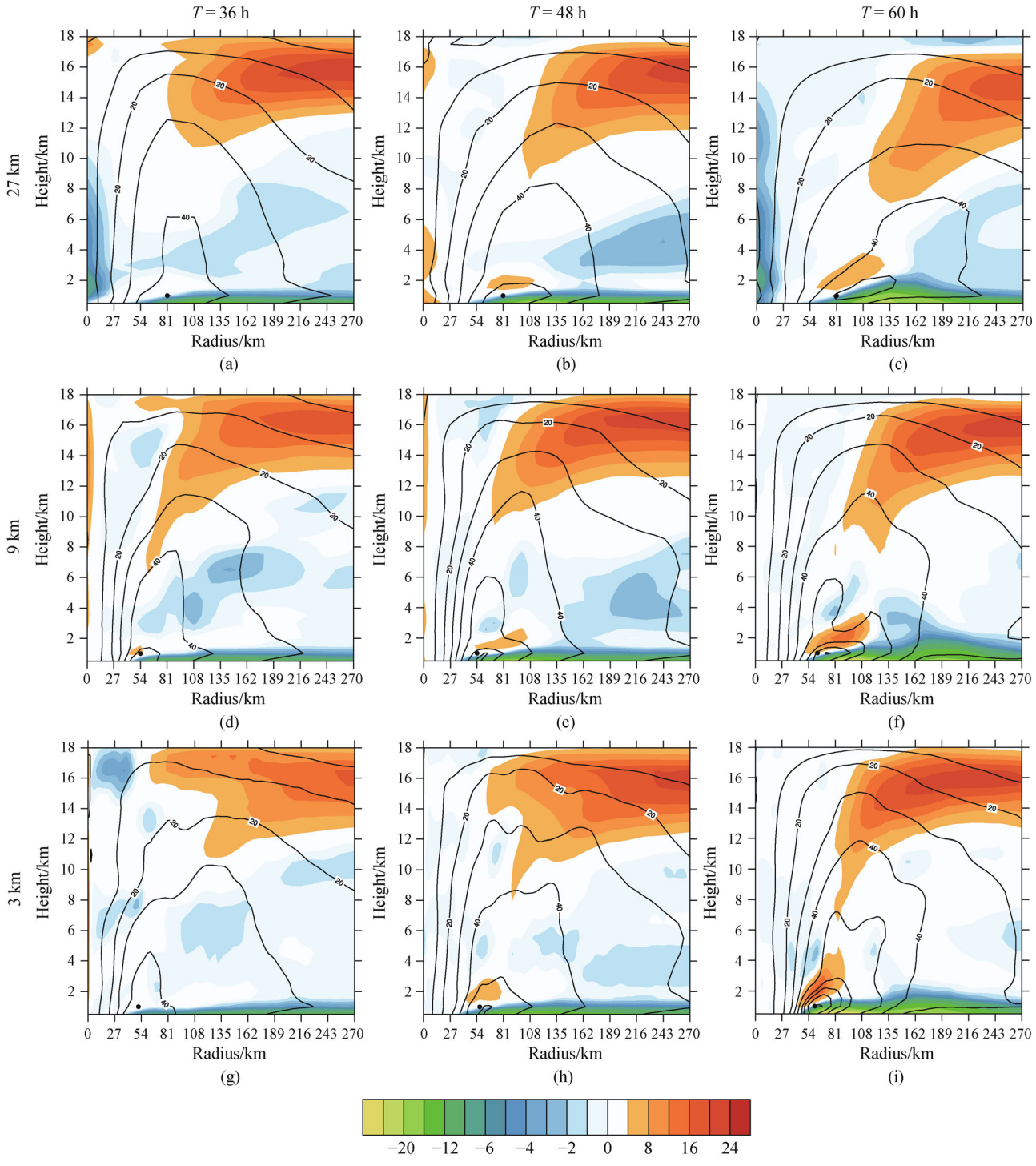

Fig. 10 The radius-height plots of axisymmetric tangential wind speed (contoured, units: m/s) and radial wind speed (shaded, units: m/s) in (a)–(c) EXP_27, (d)−(f) EXP_9 and (g)−(i) EXP_3, respectively. (Columns 1) at $T = 36$ h, (Columns 2) at $T = 48$ h and (Columns 3) at $T = 60$ h. The dots denote the radius of maximum tangential wind.

tangential winds outside the RMW in the inner-core is corresponding to larger AAM. With the addition of stronger and deeper radial inflow, more AAM would be transported inward in low-level, accounting for the enhancement of tangential flows and favor the intensification at later times. The initial inner-core tropospheric moisture conditions also affect the predictability of peak intensity. More sufficient initial inner-core moisture corresponds to stronger TC intensity at 48 h through the development of the inner-core convection. The TC

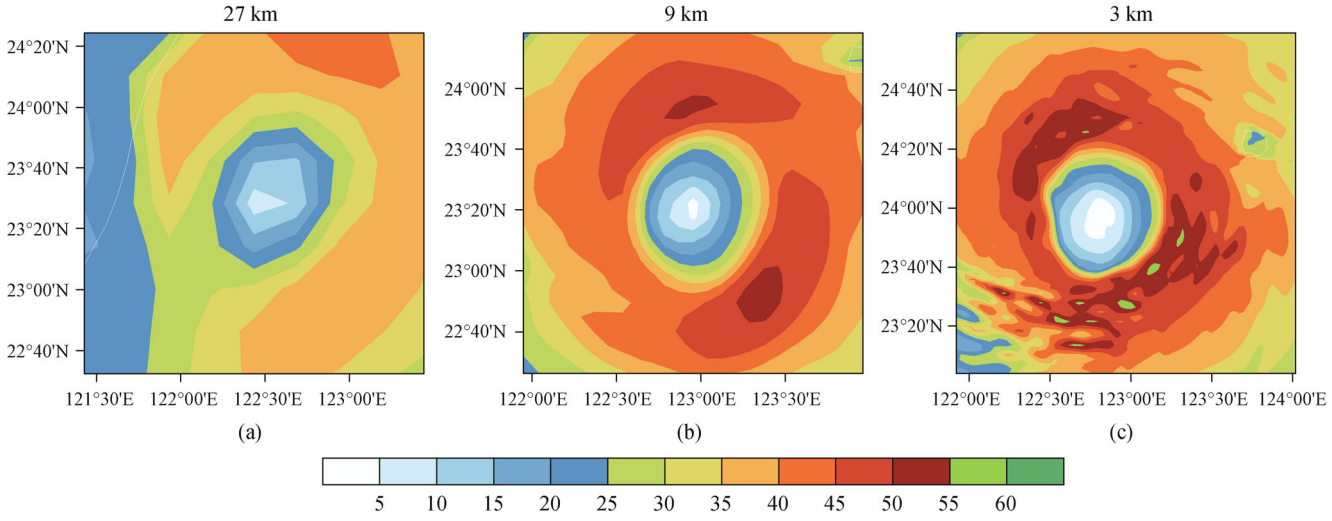

Fig. 11 Horizontal 10-m wind at 60 h in (a) EXP_27, (b)EXP_9, and (c)EXP_3 (units: m/s).

intensification is related to the aggregation and merger of convection, which is influenced by both radial advection and gradient of system-scale vortex vorticity. Stronger inflow is conducive to the inward advection of the convection. More intensive tangential wind and radial wind in the inner-core is corresponding to denser vorticity gradient, which is beneficial to the collecting of the small-scale convection and thus the intensification of system-scale TC.

Besides the IC uncertainty, model uncertainty is also noteworthy. According to the sensitivity experiments, horizontal grid resolution plays an important role on the predictability of Lekima's intensity when observed intensity is greater than 40 m/s in the current simulations. The forecast errors of peak intensity in EXP_3 have been reduced by 90% compared to EXP_9, and 95% to EXP_27, demonstrating the positive effect of improving resolution on peak intensity forecast. In EXP_3, the vortex structure is more compact and the radial gradient of horizontal wind is extremely larger than the other two, yielding to stronger peak intensity. Overall, the model uncertainty in terms of model resolution greatly impacts the predictability of Lekima's intensity, the finer resolution is crucial to simulate the intensification and capture the observed peak value.

This manuscript demonstrates the role of the initial condition in inner-core and model resolution, suggesting the importance of inner-core data assimilation and a high-resolution model. However, it is worth stressing that these two factors only account for part of error sources associated with intensity predictability. Other factors including initial condition in environmental fields and model physics may also be crucial, which will be investigated in our future studies.

Acknowledgements The authors would like to thank Dr. Li-na Bai in STI for providing the best-track data. This research was primarily supported by National Key R&D Program of China (No. 2018YFC1506404), National Natural Science Foundation of China (Grant No. 41575107), and in part by Shanghai Sailing Program (No. 19YF1458700), the Research Program from Science and Technology Committee of Shanghai (No. 19dz1200101), and Science and Technology Project of Shanghai Meteorological Service (No. QM202006) , and Typhoon Scientific and Technological Innovation Group of Shanghai Meteorological Service.

Electronic Supplementary material is available in the online version of this article at http://dx.doi.org/10.1007/s11707-021-0877-x and is accessible for authorized users.

References

Andreas E L, Mahrt L (2016). On the prospects for observing spray-mediated air-sea transfer in wind-water tunnels. J Atmos Sci, 73(1): 185–198

Berner J, Fossell K R, Ha S Y, Hacker J P, Snyder C (2015). Increasing the skill of probabilistic forecasts: understanding performance improvements from model-error representations. Mon Weather Rev, 143(4): 1295–1320

Carrasco C A, Landsea C W, Lin Y L (2014). The influence of tropical cyclone size on its intensification. Weather Forecast, 29(3): 582–590

Chan K T F, Chan J C L (2013). Angular momentum transports and synoptic flow patterns associated with tropical cyclone size change. Mon Weather Rev, 141(11): 3985–4007

Chen D Y C, Cheung K K W, Lee C S (2011). Some implications of core regime wind structures in western north pacific tropical cyclones. Weather Forecast, 26(1): 61–75

Chen P Y, Yu H, Xu M, Lei X T, Zeng F (2019). A simplified index to assess the combined impact of tropical cyclone precipitation and wind on China. Front Earth Sci, 13(4): 672–681

DeMaria M, Sampson C R, Knaff J A, Musgrave K D (2014). Is tropical cyclone intensity guidance improving? Bull Am Meteorol Soc, 95(3): 387–398

Emanuel K, Zhang F (2017). The role of inner-core moisture in tropical cyclone predictability and practical forecast skill. J Atmos Sci, 74(7): 2315–2324

Ge X, Li T, Peng M S (2013). Tropical cyclone genesis efficiency: mid-level versus bottom vortex. J Trop Meteorol, 19(3): 197–213

Gentry M S, Lackmann G M (2010). Sensitivity of simulated tropical cyclone structure and intensity to horizontal resolution. Mon Weather Rev, 138(3): 688–704

Gray W M (1998). The formation of tropical cyclones. Meteorol Atmos Phys, 67(1-4): 37–69

Guo X, Tan Z M (2017). Tropical cyclone fullness: a new concept for interpreting storm intensity. Geophys Res Lett, 44(9): 4324–4331

Hong S Y, Dudhia J, Chen S H (2004). A revised approach to ice microphysical processes for the bulk parameterization of clouds and precipitation. Mon Weather Rev, 132(1): 103–120

Hong S Y, Noh Y, Dudhia J (2006). A new vertical diffusion package with an explicit treatment of entrainment processes. Mon Weather Rev, 134(9): 2318–2341

Jin H, Peng M S, Jin Y, Doyle J D (2014). An evaluation of the impact of horizontal resolution on tropical cyclone predictions using COAMPS-TC. Weather Forecast, 29(2): 252–270

Kain J S, Fritsch J M (1993). Convective parameterization for mesoscale models: the Kain-Fritsch scheme. The Representation of Cumulus Convection in Numerical Models, Meteor Monogr, No. 46, Amer Meteor Soc, 165–170

Liu S, Tao D, Zhao K, Minamide M, Zhang F (2018). Dynamics and predictability of the rapid intensification of Super Typhoon Usagi (2013). J Geophys Res Atmos, 123: 7462–7481

Montgomery M T, Nicholls M E, Cram T A, Saunders A B (2006). A vortical hot tower route to tropical cyclogenesis. J Atmos Sci, 63(1): 355–386

Munsell E B, Zhang F, Sippel J A, Braun S A, Weng Y (2017). Dynamics and predictability of the intensification of Hurricane Edouard (2014). J Atmos Sci, 74(2): 573–595

Nguyen S V, Smith R K, Montgomery M T (2008). Tropical-cyclone intensification and predictability in three dimensions. Q J R Meteorol Soc, 134(632): 563–582

Nystrom R G, Zhang F, Munsell E B, Braun S A, Sippel J A, Weng Y, Emanuel K (2018). Predictability and dynamics of hurricane Joaquin (2015) explored through convection permitting ensemble sensitivity experiments. J Atmos Sci, 75(2): 401–424

Nystrom R G, Zhang F (2019). Practical uncertainties in the limited predictability of the record-breaking intensification of hurricane Patricia (2015). Mon Weather Rev, 147(10): 3535–3556

Roberts M J, Camp J, Seddon J, Vidale P L, Hodges K, Vanniere B, Mecking J, Haarsma R, Bellucci A, Scoccimarro E, Caron L P, Chauvin F, Terray L, Valcke S, Moine M P, Putrasahan D, Roberts C, Senan R, Zarzycki C, Ullrich P (2020). Impact of model resolution on tropical cyclone simulation using the HighResMIP–PRIMAVERA multimodel ensemble. J Clim, 33(7): 2557–2583

Rogers R F (2010). Convective-scale structure and evolution during a high-resolution simulation of tropical cyclone rapid intensification. J Atmos Sci, 67(1): 44–70

Rogers R F, Zhang J A, Zawislak J, Jiang H, Alvey G R III, Zipser E J, Stevenson S N (2016). Observations of the structure and evolution of hurricane Edouard (2014) during intensity change. Part II: kinematic structure and the distribution of deep convection. Mon Weather Rev, 144(9): 3355–3376

Ryglicki D R, Doyle J D, Jin Y, Hodyss D, Cossuth J H (2018). The unexpected rapid intensification of tropical cyclones in moderate vertical wind shear. Part II: vortex tilt. Mon Weather Rev, 146(11): 3801–3825

Schecter D A, Dubin D H (1999). Vortex motion driven by a background vorticity gradient. Phys Rev Lett, 83(11): 2191–2194

Sippel J A, Zhang F (2008). A probabilistic analysis of the dynamics and predictability of tropical cyclogenesis. J Atmos Sci, 65(11): 3440–3459

Skamarock W C, Coauthors (2008). A description of the Advanced Research WRF version 3. NCAR Tech. Note NCAR/TN-475 + STR

Tao D, Zhang F (2014). Effect of environmental shear, sea-surface temperature, and ambient moisture on the formation and predictability of tropical cyclones: an ensemble-mean perspective. J Adv Model Earth Syst, 6(2): 384–404

Tao D, Zhang F (2015). Effects of vertical wind shear on the predictability of tropical cyclones: practical versus intrinsic limit. J Adv Model Earth Syst, 7(4): 1534–1553

Vannière B, Roberts M, Vidale P L, Hodges K, Demory M E, Caron L P, Scoccimarro E, Terray L, Senan R (2020). The moisture budget of tropical cyclones in HighResMIP models: large-scale environmental balance and sensitivity to horizontal resolution. J Clim, 33(19): 8457–8474

Wang Y (2009). How do outer spiral rainbands affect tropical cyclone structure and intensity? J Atmos Sci, 66(5): 1250–1273

Wang Y, Heng J (2016). Contribution of eye excess energy to the intensification rate of tropical cyclones: a numerical study. J Adv Model Earth Syst, 8(4): 1953–1968

Xu J, Wang Y (2010). Sensitivity of the simulated tropical cyclone inner-core size to the initial vortex size. Mon Weather Rev, 138(11): 4135–4157

Xu M, Zhou S, Ge X (2016). An idealized simulation study of the impact of monsoon gyre on tropical cyclogenesis. Acta Meteorol Sin, 74(5): 733–743

Ying M, Zhang W, Yu H, Lu X, Feng J, Fan Y, Zhu Y, Chen D (2014). An overview of the China meteorological administration tropical cyclone database. J Atmos Ocean Technol, 31(2): 287–301

Yu H, Chen L S (2019). Impact assessment of landfalling tropical cyclones: introduction to the special issue. Front Earth Sci, 13(4): 669–671

Zhang F, Tao D (2013). Effects of vertical wind shear on the predictability of tropical cyclones. J Atmos Sci, 70(3): 975–983

Zhang F, Sippel J A (2009). Effects of moist convection on hurricane predictability. J Atmos Sci, 66(7): 1944–1961